Available online at www.sciencedirect.com
SCIENCE DIRECT
Thin Solid Films 491 (2005) 38 – 42
thin solid films
www.elsevier.com/locate/tsf

Optical and electrical properties of self-assembled, ordered gold nanocrystal/silica thin films prepared by sol–gel processing☆

Kai Yang [a], Hongyou Fan [b], Kevin J. Malloy [a], C. Jeffrey Brinker [c,d], Thomas W. Sigmon [a,*]

[a] Center for High Technology Materials, the University of New Mexico, Albuquerque, NM 87106, USA
[b] Ceramic Processing and Inorganic Materials Department, Advanced Materials Laboratory, Sandia National Laboratories, Albuquerque, NM 87106, USA
[c] Self-Assembled Materials Department, Advanced Materials Laboratory, Sandia National Laboratories, Albuquerque, NM 87106, USA
[d] Department of Chemical and Nuclear Engineering, the University of New Mexico, Albuquerque, NM 87106, USA

Received 11 January 2005; received in revised form 27 April 2005; accepted 3 May 2005
Available online 15 July 2005

Abstract

Highly ordered gold nanocrystal (NC)/silica films are synthesized by self-assembly of water-soluble gold NC micelles and silica using a sol–gel spin coating technique. The optical properties are analyzed using ellipsometry and ultraviolet-visible spectroscopy. Transmission and absorption spectra were measured for wavelengths ranging from 200 to 2000 nm. The absorption spectra show a strong surface plasmon absorption band at ~520 nm for all samples. Charge transport behavior of the films was examined using metal-oxide-semiconductor (MOS) and metal-insulator-metal (MIM) structures. MOS capacitor samples exhibit charge storage with discharge behavior dominated by electron transport within the gold NC arrays. Low temperature current–voltage measurements on MIM devices reveal electrical conduction with a thermal activation energy of ~90 meV. For temperatures less than 100 K, the $I-V$ characteristics of the NC film exhibits a strong coulomb blockade effect, with a threshold voltage of ~0.5 V measured at 78 K.

Keywords: Gold; Nanostructures; Optical properties; Electrical properties and measurements

1. Introduction

Nanometer-sized crystallites of metals, semiconductors, and oxides form a new class of "artificial solids" possessing electrical properties far different from those of either the corresponding isolated atoms or macroscopic solids [1–4]. The ability to adjust the properties of such solids through control of the size, shape, composition, crystallinity, and structure of the crystallites leads to a wide range of potential applications. For instance, memory-cell structures employing metal nanocrystals (NC) as the charge storage media have been under investigation as promising candidates for replacing conventional dynamic random access memory or flash memories [5,6]. Recently, we demonstrated direct synthesis of water-soluble nanocrystalline gold micelles, including their self-assembly with silica into robust, ordered, nanocrystalline arrays in bulk or thin film forms [1,7]. These ordered arrays of metallic nanocrystals are potential implementations of several types of model systems including the nanocrystal memory devices mentioned above [6].

In this work, we report the electrical and optical properties of highly ordered gold NC/silica films. The films are synthesized through self-assembly of water-soluble gold NC micelles and soluble silica by sol–gel processing. Their optical properties are analyzed with ellipsometry and ultraviolet (UV)-visible spectroscopy. Transmission and absorption spectra were measured from 200 to 2000 nm using a Perkin-Elmer photospectrometer. The absorption

☆ This work was supported by the U.S. Department of Energy (DOE) Basic Energy Sciences Program, the Air Force Office of Scientific Research, and the Army Research Office (ARO). Sandia is a multiprogram laboratory operated by Sandia Corporation, a Lockheed Martin Company, for the United States Department of Energy's National Nuclear Security Administration under Contract DE-AC04-94AL85000.
* Corresponding author. Tel.: +1 505 272 7805; fax: +1 505 272 7806.
E-mail address: sigmon@chtm.unm.edu (T.W. Sigmon).

0040-6090/$ - see front matter © 2005 Elsevier B.V. All rights reserved.
doi:10.1016/j.tsf.2005.05.040

spectra show a strong surface plasmon resonance (SPR) absorption at ~520 nm for all samples. This result is consistent with previous results indicating that the resonance peak should exhibit a blue-shift with decreasing particle size [8,9]. Charge transport behavior of the films was examined using metal-oxide-semiconductor (MOS) and metal-insulator-metal (MIM) structures. MOS capacitor samples exhibit charge storage with discharge behavior dominated by electron transport within the gold NC arrays. Low temperature current-voltage measurements on MIM devices reveal electrical conduction with a thermal activation energy of ~90 meV. For temperatures less than 100 K, the I–V characteristics of the NC film exhibits a strong coulomb blockade effect, with a threshold voltage of ~0.5 V measured at 78 K. The formation of water-soluble NC micelles and their self-assembly into ordered 3D mesophases provides a new means to integrate model 3D NC arrays into robust devices. The NC arrays we describe could be the ideal media for the study of the Hubbard Hamiltonian and the variety of transport and collective phenomena predicted to occur for such systems.

2. Film fabrication

The gold NC/silica films are prepared by spin-coating precursor solutions onto silicon wafers of selected resistivity and carrier type [7]. The precursor solutions consist of tetraethyl orthosilicate, HCl (0.07N HCl aq.), surfactant (CTAB; $CH_3(CH_2)_{15}N^+(CH_3)Br^-$), H_2O, and gold NCs. By changing the weight percentage of gold, different gold loading factors (the amount of gold to that of silica) can be obtained for the samples. The films are coated onto the substrates by conventional spin coating using spin speeds of 500–3000 rpm in air with 10–20% relative humidity at 25 °C. Following synthesis and coating the films are cured in vacuum at 180 °C for 5 h, or in UV light for about 2 h. Typical film thicknesses range from ~30 to 300 nm for the gold NC/silica films fabricated by this approach. Transmission electron microscopy (TEM) is used to directly observe microstructures of gold NC/silica arrays. TEM is performed on a JEOL 2010 with 200 kV accelerating voltage, equipped with a Gatan slow scan charge couple device camera. Fig. 1 shows a TEM image of a [111]-oriented gold NC array along with its corresponding electron diffraction pattern. The TEM image is consistent with a face-center-cubic structure with unit cell of ~10 nm and average interparticle spacing of ~5 nm. Compared to other connected NC systems, for example, those prepared by desoxyribo nucleic acid hybridization [10], the thermodynamically controlled self-assembly process provides greater order and control of NC spacing, while the surrounding silica matrix provides greater chemical, mechanical and thermal robustness.

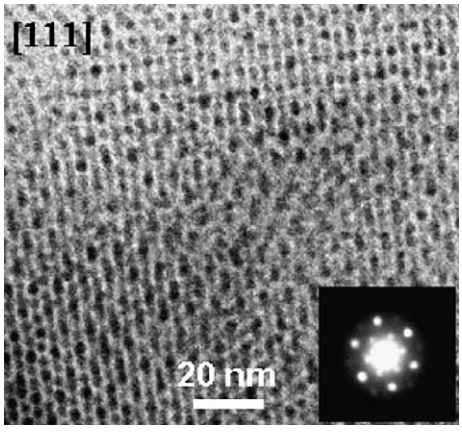

Fig. 1. TEM image of a [111]-orientated gold NC/silica film. The inset shows the corresponding electron diffraction pattern.

3. Optical experiments and discussion

The refractive index of a set of samples with different gold loading factors (0, 0.25, 0.5, and 1.0) prepared in the previously described manner (annealed at 180 °C for 5 h) was measured by ellipsometry. The film thickness of these artificial dielectric films ranged from 110 to 150 nm. Fig. 2 shows the optical refractive index of the gold NC/silica thin films as a function of the gold loading factor. The index is seen to increase with gold loading factor varying from 1.46 to 1.70. Simple empirical formulas were obtained for the optical refractive index of these films by fitting the experimental data with both linear and polynomial fits and are shown in Fig. 2.

The surface plasmon resonance of metal nanoparticles in composites occurs in the UV-visible to near-IR spectral region, depending on the metal species, nanoparticle shape, size, and the incorporating dielectric medium [11,12]. For nanocomposites comprised of gold nanoparticles in glass or solution, a SPR band around 550 nm is found [8]. In our work, we examined the films coated on glass substrates with different thicknesses (~0.15, 0.3, 0.8, 1.0, and 1.5 μm), a fixed gold NC size of ~3 nm, and a gold loading factor of 1.0. Transmission and absorption spectra from 200 to 2000 nm were measured for these films using a Perkin-Elmer UV-Visible-IR spectrometer. As can be seen, all samples exhibit a strong SPR absorption band at ~520 nm (Figs. 3 and 4), as expected from gold NCs.

4. Electrical experiments and discussions

To investigate the charge transport in these self-assembled, ordered, nanocrystal arrays, both planar MOS and MIM devices were fabricated using either a silica or gold NC/silica mesophase 'oxide'. Both MOS and MIM devices are fabricated on (100) p-type silicon wafers of $\sim 10^{15}$ cm^{-3} doping concentration. For the MOS devices, following standard cleaning procedures, backside metal

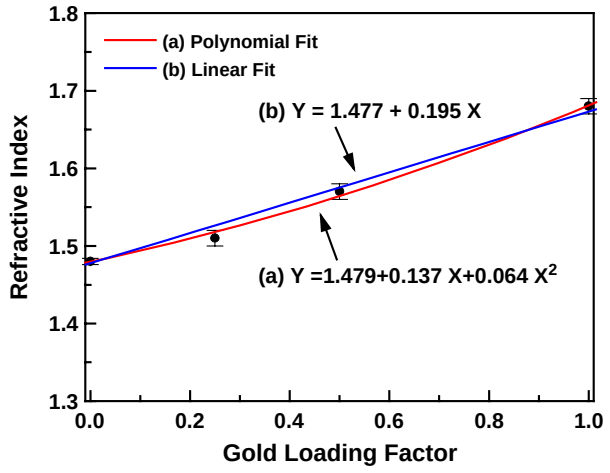

Fig. 2. Dependence of the refractive index of Au NC/silica films on gold loading factor. The gold loading factor is defined by the amount of gold to that of silica. The results of a linear fit, ($Y=1.447+0.195X$) where Y is the refractive index, and X the gold loading factor is shown. A better fit is obtained by adding a bowing factor, shown in the curve for $Y=1.479+0.137X+0.064X^2$.

contacts were deposited (400 nm of e-beam evaporated Al) and annealed in forming gas at 450 °C for 25 min. For the MIM devices, the wafers are first thermally oxidized to a thickness of 200 nm, and then a 400 nm thick Al electrode is deposited onto this oxide. Gold NC/silica films, approximately 100-nm thick, are then deposited on the surface of all wafers by spin-coating. The films are then annealed in *UV* light at room temperature for 1.5 h to remove organics and promote additional siloxane condensation. The top contact pads for both MOS and MIM devices are then formed by *e*-beam evaporation of Al (~400 nm) through a shadow mask. Control samples were fabricated by spin-coating gold-free silica sols designed to form silica layers comparable to those of the silica matrices of the gold NC/silica films.

High frequency capacitance–voltage (C–V), current–voltage (I–V) and charge storage measurements were then performed on the MOS structures at room temperature. C–

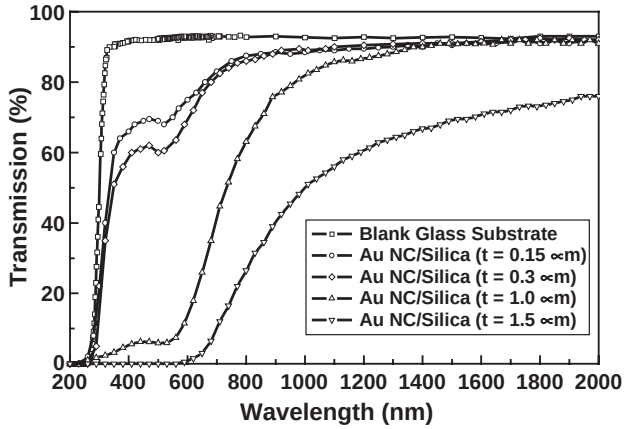

Fig. 3. Optical transmission spectra of the gold NC/silica films for various film thicknesses. A drop in transmission is observed around 520 nm.

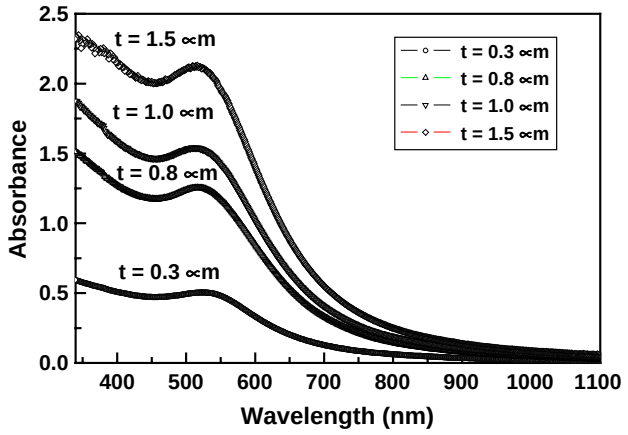

Fig. 4. Optical absorption spectra of the gold NC/silica films for various film thicknesses. The films exhibit a characteristic surface plasmon resonance band at ~520 nm, as expected from gold NCs.

V measurements were obtained using either a SULA Technology DLTS Spectrometer driven by a Stanford Research DS345 function generator or a Keithley System 82-WIN C–V analyzer. Temperature-dependent I–V characteristics are measured on the MIM samples. For these measurements, the sample is mounted on an MMR cold finger in a vacuum of less than 2×10^{-6} torr, and cooled to low temperatures. DC current–voltage measurements are made using a HP 4140B picoammeter or HP 4155B semiconductor parameter analyzer and the temperature is varied from 300 to 77 K using a Lakeshore 330 auto tuning temperature controller.

In Fig. 5, we plot the results of electric field-aided transport and charge storage measurements performed on the MOS capacitors for both types of silica films (with and without gold NCs). In this measurement the sample is

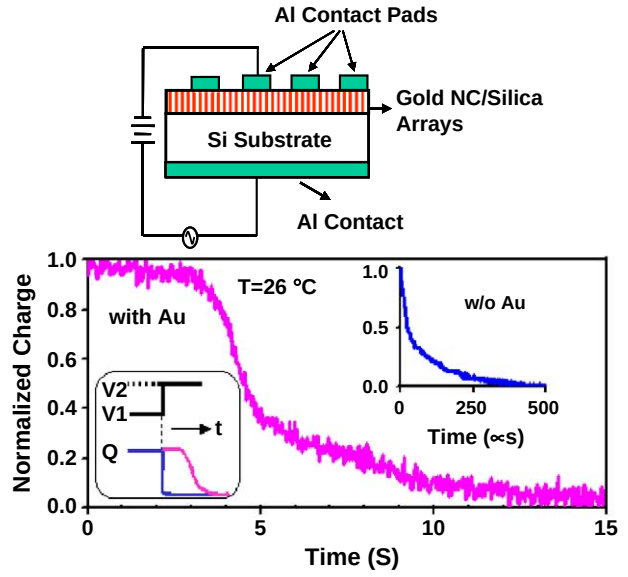

Fig. 5. Transient charge measurements on MOS capacitors prepared using silica or gold NC/silica as the 'oxide' dielectrics. A cross-section of the capacitor is shown.

initially biased at $V_1 = -2$ V for 50 s, then rapidly switched to $V_2 = 2$ V (<1 μs) and the time evolution of the capacitor charge monitored. Samples without gold exhibit an exponential discharge (~100 μs) (inset Fig. 5) consistent with normal *RC* discharge behavior. For the samples with gold, an ogive (S-shaped) profile with a ~7.5 s (10% to 90% points) discharge time is observed. We calculate the total excess charge contained in this capacitor to be approximately 3×10^{-11} C corresponding to 1×10^{18} cm^{-3} NCs occupied with electrons. We attribute this to the charging of the gold NCs in the oxide near the gate electrode when the gate is negatively biased. Upon reversing the gate voltage to V_2, electrons on the gold NCs are swept out of the oxide into the gate sequentially from the gate side first. No change in substrate capacitance occurs until the gold NCs in the oxide are discharged as they effectively pin the Si-surface in accumulation. We estimate a uniform gold NC concentration in the oxide of $\sim 4 \times 10^{18}$ cm^{-3}. However, only those NCs located near the gate electrode can respond to the high frequency ac-signal used to measure the capacitance, resulting in roughly all of the NCs in the first 25% of the oxide film being occupied by electrons. Given the spacing for these dots, we expect that coulomb blockade effects [13,14] are important in the carrier transport amongst the gold NCs. In that we observe charge storage and transport behavior that is *completely different* from the corresponding MOS capacitor prepared without gold using a silica gate oxide identical to that of the host matrix of the NC array, it is evident that charge is stored on the Au NCs and that the discharge characteristics are dominated by electron transport involving the nanocrystals.

To further elucidate the transport properties of the gold NC arrays, low temperature *I–V* measurements were performed using the MIM samples. In Fig. 6, the *I–V* curves are plotted at temperatures from 300 to 78 K. For room temperature, the *I–V* curve is seen to be linear with a zero-biased resistance of ~14 MΩ, corresponding to a film resistivity of about 3×10^6 ohm-cm. Nonlinearity in the *I–V*

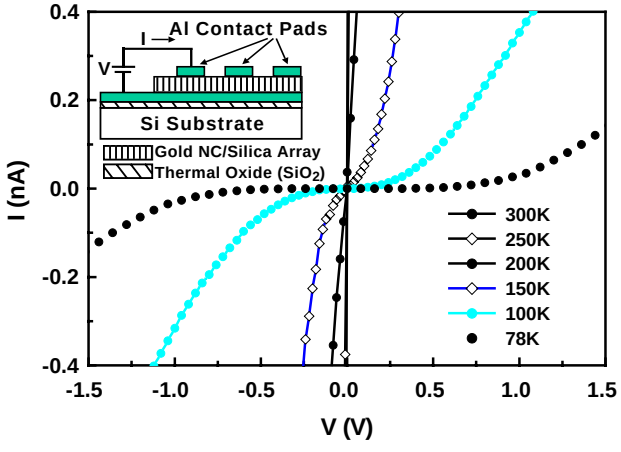

Fig. 6. Measured *I–V* curves at temperatures from 300 to 78 K for the MIM devices. A cross-section of a MIM device is shown.

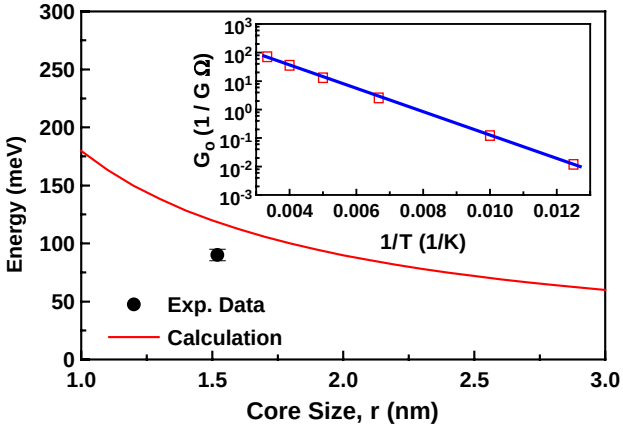

Fig. 7. Calculated coulomb charging energy as a function of core size of the gold nanocrystal. The inset shows the Zero-bias conductance (G_0) versus $1/T$ derived from our temperature dependent *I–V* measurements.

behavior near zero bias becomes evident at ~200 K and increases with decreasing temperature. At 78 K, a finite threshold voltage, V_T, is required to generate current through the gold NC/silica insulator, indicative of coulomb blockade behavior, resulting from electrical isolation of the NCs. By comparison, measurements on gold-free control samples show *no significant change* in the *I–V* characteristics over this temperature range.

The temperature dependence of the zero bias conductance (G_0) is shown in Fig. 7 (inset) as an Arrhenius plot [$\log(G_0)$ vs. $1/T$]. The activation energy derived from the slope of this plot (90.4 meV) provides information on the transport properties of the layer. We expect low voltage electron transport through an array of Coulomb islands to be dominated by the energy required to electrically charge the individual islands. Models of electrical conduction in such an array of identical metal islands predict a thermally activated behavior $G_0 \exp[-E_a/k_B T]$ where E_a is the

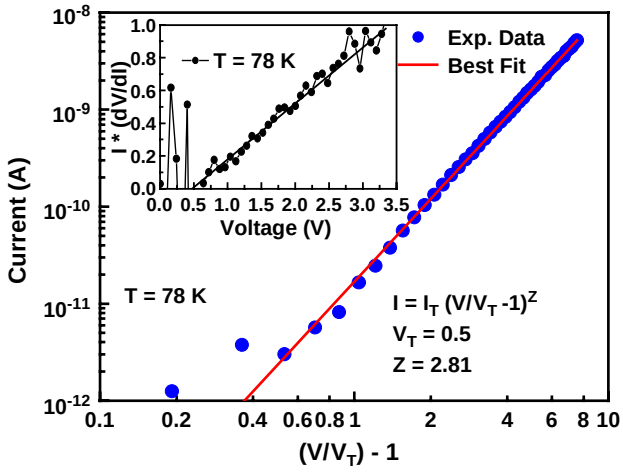

Fig. 8. Scaling behavior of the *I–V* characteristics at 78 K. The exponent, *z*, is determined by a best fit using the scaling formula, and for the device shown is 2.81. The inset shows the measured threshold voltage of ~0.5V at 78K.

activation energy to charge an electrically neutral nanocrystal and k_B is Boltzmann's constant. The coulomb charging energy equals $e^2/2C_0$, where $C_0=4\pi\varepsilon\varepsilon_0 r$, the capacitance of an isolated NC, depends on the dielectric constant of the surrounding medium ε and the nanocrystal radius r. For an isolated metal nanocrystal of radius $r \sim 1.5$ nm surrounded by a medium of dielectric constant $\varepsilon = 3.9$, the Coulomb energy is as high as $\sim$ 123 meV, for $C_0=4\pi\varepsilon\varepsilon_0 r=0.7$ aF. The Coulomb charging energy calculated from the isolated model is plotted as a function of the core size of the nanocrystal (r, radius) in Fig. 7. It should be pointed out that this calculation ignores the weak coupling between the gold nanoparticle and its nearest neighbors, and therefore slightly over estimates the value of E_a. The experimental determination of $E_a=90.4$ meV (Fig. 7) agrees well with the calculated values of 123 meV for our gold nanocrystal particle sizes of $r=\sim 1.5$ nm.

At low temperatures, all samples show a clear voltage threshold for conduction, indicating strong coulomb blockade behavior at ~78 K. In one particular device, a threshold voltage of ~0.5 V was measured at 78 K. The voltage dependence of current (for $V>V_T$) depends on the number of current paths accessible through the gold nanocrystal arrays [15]. Theory [16] predicts the current through a uniform array of nanodots to follow $I=I_0(V/V_T-1)^z$ (for $V>V_T$), where z is a scaling exponent that depends on array dimensionality. For our gold nanocrystal devices we obtained a value for z of ~2.81 (Fig. 8), implying a quasi 3-D nanocrystal film.

5. Conclusions

In conclusion, we report optical and electrical results on highly ordered gold NC/silica films. We examined films having different gold NC/silica film thicknesses with fixed gold NC size of ~3 nm. The absorption spectra show a strong SPR absorption band at ~520 nm for all samples, as expected from gold NCs. Charge transport behavior of self-assembled ordered gold NC/silica arrays has been measured for the first time. Experiments on MOS capacitors exhibit charge storage and discharge behavior dominated by electron transport within the ordered NC arrays. Low temperature $I-V$ measurements on MIM samples reveal that electrical conduction in the film has a thermal activation energy of 90.4 meV, in good agreement with theoretical predictions. At low temperatures (< 100K), the $I-V$ curves become nonlinear near zero bias, exhibiting strong coulomb blockade effects with a threshold voltage of about 0.5 V measured at 78 K.

References

[1] C.J. Brinker, MRS Bulletin ((2004) September) 631.
[2] R.P. Andres, J.D. Bielefeld, J.I. Henderson, D.B. Janes, V.R. Kolagunta, C.P. Kubiak, W.J. Mahoney, R.G. Osifchin, Science 273 (1996) 1690.
[3] C.T. Black, C.B. Murray, R.L. Sandstrom, S.H. Sun, Science 290 (2000) 1131.
[4] A. Bezryadin, R.M. Westervelt, M. Tinkham, Appl. Phys. Lett. 74 (1999) 2699.
[5] S. Tiwari, F. Rana, H. Hanafi, A. Hartstein, E.F. Crabbe, K. Chan, Appl. Phys. Lett. 68 (1996) 1377.
[6] Z. Liu, C. Lee, V. Narayanan, G. Pei, E.C. Kan, IEEE Trans. Electron Devices 49 (2002) 1606.
[7] H.Y. Fan, K. Yang, D.M. Boye, T.W. Sigmon, K.J. Malloy, C.J. Brinker, H. Xu, Science 304 (2004) 567.
[8] S. Qu, H. Li, T. Peng, Y. Gao, J. Qiu, C. Zhu, Mater. Lett. 58 (2004) 1427.
[9] U. Kreibig, L. Genzel, Surf. Sci. 156 (1985) 678.
[10] C.A. Mirkin, R.L. Letsinger, R.C. Mucic, J.J. Storhoff, Nature 382 (1996) 607.
[11] W.L. Barnes, A. Dereux, T.W. Ebbesen, Nature 424 (2003) 824.
[12] S. Debrus, J. Lafait, M. May, N. Pincon, D. Prot, C. Sella, J. Venturini, J. Appl. Phys. 88 (8) (2000) 4469.
[13] H. Grabert, M.H. Devoret, Single Charge Tunneling, Plenum Press, New York, 1992.
[14] M.G. Ancona, W. Kruppa, R.W. Rendell, A.W. Snow, D. Park, J.B. Boos, Phys. Rev., B 64 (2001) 33408.
[15] R. Parthasarathy, X.M. Lin, H.M. Jaeger, Phys. Rev. Lett. 87 (2001) 6807.
[16] A.A. Middleton, N.S. Wingreen, Phys. Rev. Lett. 71 (1993) 3198.